Available online at www.sciencedirect.com
ScienceDirect
Journal of Sound and Vibration 320 (2009) 1–15
JOURNAL OF SOUND AND VIBRATION
www.elsevier.com/locate/jsvi

Design and optimization of input shapers for liquid slosh suppression

Ameen Aboel-Hassan, Mustafa Arafa*, Ashraf Nassef

Mechanical Engineering Department, American University in Cairo, Cairo, Egypt

Received 10 January 2008; received in revised form 16 July 2008; accepted 22 July 2008
Handling Editor: C.L. Morfey
Available online 30 August 2008

Abstract

The need for fast maneuvering and accurate positioning of flexible structures poses a control challenge. The inherent flexibility in these lightly damped systems creates large undesirable residual vibrations in response to rapid excitations. Several control approaches have been proposed to tackle this class of problems, of which the input shaping technique is appealing in many aspects.

While input shaping has been widely investigated to attenuate residual vibrations in flexible structures, less attention was granted to expand its viability in further applications. The aim of this work is to develop a methodology for applying input shaping techniques to suppress sloshing effects in open moving containers to facilitate safe and fast point-to-point movements. The liquid behavior is modeled using finite element analysis. The input shaper parameters are optimized to find the commands that would result in minimum residual vibration. Other objectives, such as improved robustness, and motion constraints such as deflection limiting are also addressed in the optimization scheme. Numerical results are verified on an experimental setup consisting of a small motor-driven water tank undergoing rectilinear motion, while measuring both the tank motion and free surface displacement of the water. The results obtained suggest that input shaping is an effective method for liquid slosh suppression.

1. Introduction

The response of lightly damped flexible structures to rapid excitations, as in point-to-point maneuvering, usually entails large undesirable residual vibrations which may degrade the positioning accuracy and may even be severe enough to cause safety hazards, as in the transport of molten metal in ladles, for instance. In gantry cranes, one way to maintain vibrations within tolerable limits is to drive these systems at low speeds, often lower than the capability of their motors only to limit the sway of the payload. In other applications, considerable time can be wasted in waiting for residual vibrations to die out before the next motion command can safely be issued.

*Corresponding author. Tel.: +202 2797 5789; fax: +202 2795 7565.
E-mail address: mharafa@aucegypt.edu (M. Arafa).

0022-460X/$ - see front matter © 2008 Elsevier Ltd. All rights reserved.
doi:10.1016/j.jsv.2008.07.015

Numerous techniques are reported in the literature addressing the control of flexible structures to produce fast and accurate maneuvering while damping their undesirable dynamics, of which the input shaping technique is attractive in many aspects and hence will be the focus of the present study. Input shaping—also known as command shaping—has received considerable attention since its formal introduction by the seminal work of Singer and Seering [1]. The method proved successful in reducing residual vibrations in flexible structures such as gantry cranes and satellite antennas. The main idea behind input shaping is utilizing the flexible modes of the system to cancel residual vibration by convolving the reference command with a set of self-destructive impulses to achieve the desired motion while maintaining a low level of residual vibration at the end of the control command. One main advantage of input shaping is that no sensor feedback is required. However, the method can be sensitive to modeling errors and parameter variation. This has prompted research into enhancing insensitivity [1–3] and utilizing adaptive input shaping [4–6]. Other research fronts include incorporation of the system nonlinearities in the shaper design [7–9], hybridization of input shaping with other control techniques [10–12], the addition of motion constraints [6,13] and the application of input shaping to novel systems and models [14–17]. While the structure and implementation of input shaping resembles conventional filters, the design of the input shaper is based on decaying sinusoids rather than the frequency domain techniques generally used for traditional filter design [18], including finite impulse response and infinite impulse response (IIR) filters.

While input shaping has extensively been investigated to attenuate residual vibrations in flexible structures, less attention was granted to expand its viability in further applications, particularly problems involving fluid–structure interaction. In this context, we mention the work of Terashima and Yano [16] who applied the technique to reduce the sloshing of molten metal in the tilting ladle of a casting production line during the forward and backward motions of the pouring cycle. The fluid was modeled by both a representative pendulum-damper model and a distributed parameter model. An optimal control law was added to compensate for the control performance of the input shaper in response to the change in the system natural frequency due to the change in the fluid level. However, the practicality of the feedback loop was questioned because of the difficulty in sensing the molten metal level in real time. Therefore, it was recommended to study the robustness of the shaper to changes in the liquid level, and to investigate the effect of the higher order modes that are likely to be excited in faster tilting motions, which in turn may affect the shaper design. It is noted that no nonlinearities were included in the design procedure. Reference is also made to the work of Feddema et al. [17] which addressed slosh suppression in moving tanks by input shaping using an IIR filter to control the acceleration profile of a robot arm based on a simple pendulum model. A double pendulum model was also utilized where the tank can be tilted during the translational movement to achieve a slosh-free motion.

While simplified equivalent mechanical models of sloshing have successfully been employed due to ease of the control design, these models cannot capture the multi-modal response of the liquid to commanded step inputs, and rely on the assumption that the liquid behaves in its fundamental mode predominantly. The aim of this paper is to further improve the use of input shaping techniques to reduce sloshing of liquids in moving containers in several aspects. First, the paper addresses achieving improved robustness through the input shaper design, as well as imposing displacement constraints to limit the sloshing motion of the liquid free surface within certain bounds to prevent spilling during maneuvers. Second, the paper accounts for significant system nonlinearities encountered in practice, including actuator saturation and friction, that can significantly alter the input shaper design. Third, the liquid sloshing in the present paper is modeled through finite element analysis (FEA) to yield a numerical model, which is combined with a dynamic model of a motor-driven tank to yield a set of ordinary differential equations that describe the fluid–structure interaction. One benefit gained by employing FEA is the capability of modeling multi-modal liquid response. In addition, the use of FEA enables the prediction of the free surface displacements from the system degrees of freedom without resorting to assumptions such as the one given in Ref. [16] where the liquid free surface displacement was assumed to be a straight line in order to relate it to angular displacements of the pendulum. Adopting the present methodology enables imposing realistic constraints to the free surface displacements and facilitates handling nonlinearities. Complexities arising from the liquid response being multi-modal, in addition to the imposed deflection limits and nonlinearities, prohibit solving for the input shaper parameters in closed form. Accordingly, an optimization scheme based on a genetic algorithm (GA) is devised to obtain

the optimum commands to minimize residual vibration. Findings of the numerical model are verified experimentally.

The remainder of this paper is organized into four sections. In Section 2, a mathematical model is formulated to simulate the dynamics of the system under investigation. This model is verified experimentally on a motor-driven water tank in Section 3. A procedure using a GA is then developed in Section 4 to derive the optimum control sequence to move the tank in point-to-point maneuvers while reducing several objectives including the slosh waves and the sensitivity to modeling errors while imposing constraints regarding the free surface liquid motion. Conclusions are finally given in Section 5.

2. Dynamic model

Fig. 1 shows a schematic diagram of the system under investigation, consisting of a rigid tank mounted on a cart that is driven by a motor through a pinion that engages with a fixed rack. The tank is partially filled with liquid to a height h_0. The length and out-of-plane width of the tank are both L. The use of input shaping to provide efficient point-to-point positioning of the tank requires determining the nature of the commands to be issued to the drive motor to fulfill these motions.

2.1. FEM of fluid–structure interaction

In order to derive a dynamic model that simulates the behavior of this system, the sloshing of liquids in rigid excited tanks will first be addressed to enable the calculation of the hydrodynamic forces f_I and f_{III} acting on the tank walls and the liquid surface displacement for specified tank motion. The finite element method (FEM) is conveniently adopted for this purpose. This model will then be combined with the motor dynamics and cart positioning scheme to obtain the system dynamic model. In this way, time history plots of the motor-driven tank, together with the motion of the liquid contained inside the tank, can be evaluated by numerical integration of a set of system differential equations.

The finite element model of a partially filled rigid tank undergoing lateral base motion was presented by Arafa [19] and can conveniently be adopted for the present study. The model relies upon discretizing the liquid domain into a grid of two-dimensional four-node rectangular elements. The structural degrees of freedom are the tank wall displacements, whereas the fluid degrees of freedom can be the nodal pressures. The equations governing the dynamics of fluid–structure interaction may be reproduced from Ref. [19] as

$$\begin{aligned} &\mathbf{M}_f\ddot{\mathbf{p}}_f + \mathbf{M}\ddot{x} + \mathbf{K}_f\mathbf{p}_f = \mathbf{0} \\ &m_I\ddot{x} + \mathbf{K}_I\mathbf{p}_f = \rho f_I \\ &m_{III}\ddot{x} + \mathbf{K}_{III}\mathbf{p}_f = \rho f_{III} \end{aligned} \tag{1}$$

where $\mathbf{p}_f$ is the vector of pressures of the free surface nodes, x is the tank displacement, ρ is the liquid density, f_I, f_{III} are the hydrodynamic forces acting on the tank walls, and all other quantities pertain to the mass and stiffness matrices of the coupled liquid–tank system. Liquid damping can easily be incorporated into the

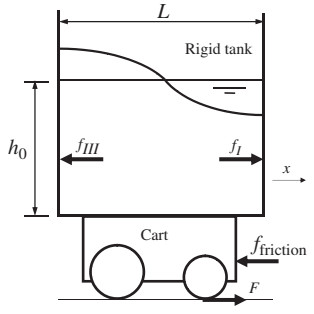

Fig. 1. Schematic diagram of cart/tank system under investigation.

model by introducing an artificial proportional damping matrix in the equations of motion having the form:

$$\mathbf{C} = \alpha \mathbf{K}_f \tag{2}$$

2.2. Motor-cart model

The block diagram in Fig. 2 shows the mathematical relations between the components of the numerical model. The input shaper block is responsible for changing the reference command into a shaped command that is designed to filter out the largest portion of the flexible modes of the system. The reference command is taken to be a step position signal in this study. The shaped command is compared with the actual position of the cart, and the error signal is fed to a proportional controller, whose output voltage signal is fed to a DC motor. The drive torque applied by the motor acts on a cart carrying a liquid-filled tank. Motion of the cart is affected by the fluid sloshing force inside the tank in addition to the force applied by the motor. The presence of the feedback is necessary for the DC motor to track the input shaper command.

The equation relating the applied voltage, V, of the DC motor to the armature current, I_m, is given by

$$V = I_m R_m + K_m K_g \frac{\dot{x}}{r} \tag{3}$$

where R_m is the armature resistance, K_m is the back emf constant, K_g is the reduction ratio of the motor gearbox and r is the output pinion radius. The torque, T, and linear force, F, generated by the motor are then given by

$$T = K_m K_g I_m = Fr \tag{4}$$

Eqs. (3) and (4) can be grouped to express the resultant motor force as a function of the applied voltage and the cart linear speed as

$$F = \frac{K_m K_g}{R_m r} V - \frac{K_m^2 K_g^2}{R_m r^2} \dot{x} \tag{5}$$

Motor saturation is included by keeping the input voltage within maximum and minimum limits. The equation governing the cart/tank dynamics can be obtained by summing all forces acting horizontally:

$$f_I - f_{III} + F - f_{\text{friction}} = M_{\text{cart}} \ddot{x} \tag{6}$$

where M_{cart} is the cart mass and f_{friction} is included in the model to account for friction forces present in the system.

2.3. System model

Eqs. (1) and (6) can be used to build a complete numerical model of the system represented by the block diagram in Fig. 2. The states of the system are taken to be the linear position and the velocity of the cart, in addition to the pressure of each node of the free liquid surface and its first derivative with respect to time, hence the system state vector is

$$\begin{Bmatrix} x_1 \\ x_2 \\ \mathbf{x}_{3\to n+3} \\ \mathbf{x}_{n+4\to 2n+4} \end{Bmatrix} = \begin{Bmatrix} x \\ \dot{x} \\ \mathbf{p}_{\mathbf{f}_{1\to n}} \\ \dot{\mathbf{p}}_{\mathbf{f}_{1\to n}} \end{Bmatrix} \tag{7}$$

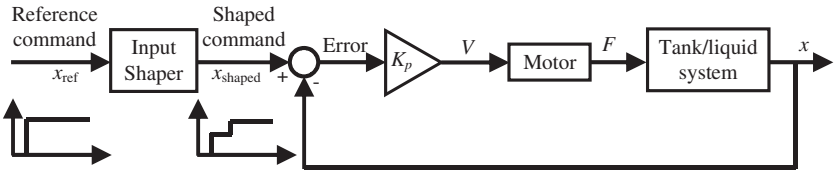

Fig. 2. Numerical model block diagram.

where n is the number of free surface nodes. The dynamic model is described by the first derivatives of the states in Eq. (7):

$$\dot{x}_1 = x_2 \tag{8}$$

where $\dot{x}_2$ can be determined by evaluating each term of the left-hand side of Eq. (6) and f_I and f_{III} can be obtained from the second and third rows in Eq. (1) as

$$\begin{aligned} f_I &= (m_I \dot{x}_2 + \mathbf{K}_I \mathbf{x}_{3\to n+3})/\rho \\ f_{III} &= (m_{III} \dot{x}_2 + \mathbf{K}_{III} \mathbf{x}_{3\to n+3})/\rho \end{aligned} \tag{9}$$

For practical applications, friction is modeled as a sliding Coulomb friction force, hence:

$$f_{\text{friction}} = -\mu N \,\text{sgn}(x_2) \tag{10}$$

where N is the normal load which is the combined weight of the tank and cart, and μ is the coefficient of kinetic friction. To account for static friction, an additional condition is added to set both the cart's velocity and acceleration to zero whenever the velocity drops below certain threshold that can be determined experimentally. This condition, together with the nonlinear sgn function in Eq. (10) can more easily be incorporated in the present numerical model than in alternate closed-form solutions.

Eqs. (5), (9) and (10) can be combined together to substitute for the left-hand side terms in Eq. (6) to solve for $\dot{x}_2$ as follows:

$$\dot{x}_2 = \frac{\rho(F - f_{\text{friction}}) + (\mathbf{K}_I - \mathbf{K}_{III})\mathbf{x}_{3\to n+3}}{(\rho M_{\text{cart}} - m_I + m_{III})} \tag{11}$$

The time derivative of the third through $n+3$ states is

$$\dot{\mathbf{x}}_{3\to n+3} = \mathbf{x}_{n+4\to 2n+4} \tag{12}$$

From Eq. (1), the time derivative of the last set of states $\mathbf{x}_{n+4\to 2n+4}$ is

$$\dot{\mathbf{x}}_{n+4\to 2n+4} = \mathbf{M}_{ff}^{-1}[\mathbf{M}\dot{x}_2 + \mathbf{K}_f \mathbf{x}_{3\to n+3}] \tag{13}$$

The time derivative of the states Eqs. (8), (11), (12) and (13) constitute the complete dynamic model that simulates the system. The displacement of the free surface nodes, $\mathbf{U}_{1\to n}$, from the undisturbed water level is given by

$$\mathbf{U}_{1\to n} = \mathbf{p}_{f_{1\to n}} \Big/ \rho g \tag{14}$$

3. Experimental work

The experimental setup shown in Fig. 3 was designed to validate the dynamic model and to study the tank/water response to optimized input shaper commands. The setup consists of a cart, driven by a DC motor, and precisely guided to undergo linear motion via linear bearings. For accurate positioning, the motor pinion meshes with a stationary rack, while the position of the cart is sensed by an optical encoder through another gear that meshes with the same rack. A partially filled water tank measuring $10 \times 10 \times 10$ cm is securely mounted on top of the cart. The water height sensor is an assembly of a float, connecting arm and optical encoder mounted on the tank wall, as shown. Because the connecting arm is directly coupled to the encoder shaft, no slippage, friction, relative motion or backlash take place, and the float was found to capture the water free surface displacement fairly accurately, especially in the low-frequency range encountered in the present study. Although input shaping does not require feeding back the water level, it still had to be measured for analysis, validation and comparison purposes. Control of the motor and the sensors feedback were handled by a personal computer using Simulink®. A block diagram of the experimental model is shown in Fig. 4. The zero vibration (ZV) input shaper is modeled using time delay, as indicated.

Fig. 5 shows a comparison of the numerical and experimental slosh responses for a commanded step input displacement. A 20×20 element mesh is used in the FE model of the liquid domain, and an artificial proportional damping matrix was added to the FE model in the form suggested by Eq. (2) with $\alpha = 0.0025$ to

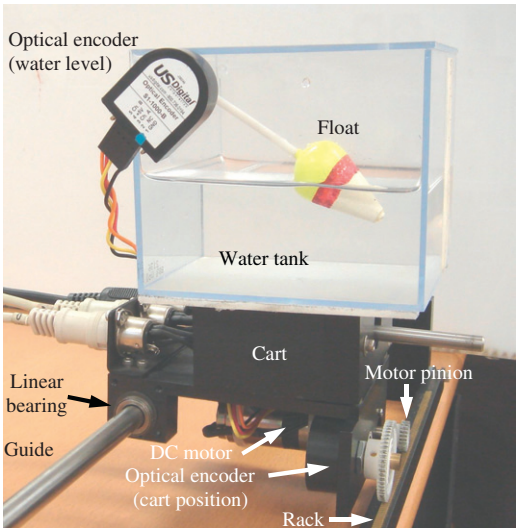

Fig. 3. Experimental setup.

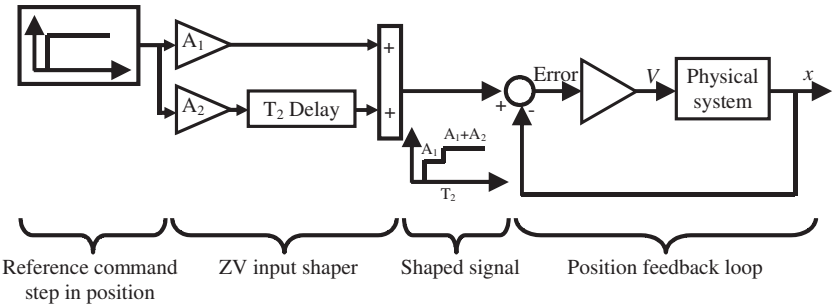

Fig. 4. Experimental model block diagram.

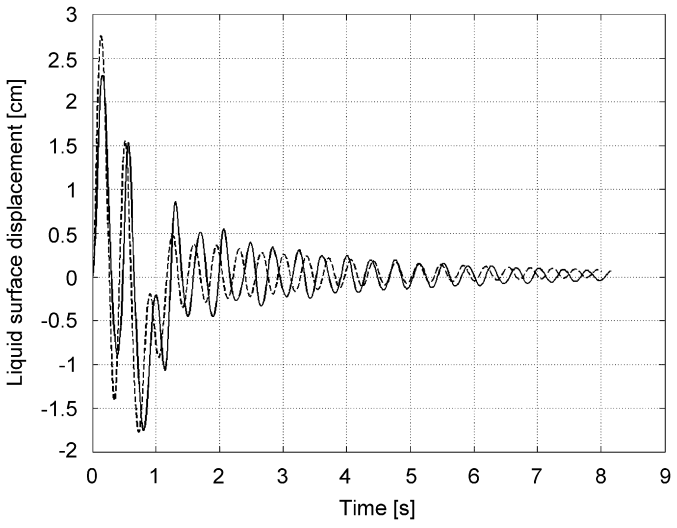

Fig. 5. Slosh response: — experimental; – – – numerical ($x_{\text{final}} = 0.6\,\text{m}$, $K_p = 25$, $h_0 = 4\,\text{cm}$).

Table 1
System parameters

Cart mass (kg)	M_{cart}	0.815
Motor armature resistance (Ω)	R_m	2.6
Back emf constant (V/rad s)	K_m	0.00767
Gearbox reduction ratio	K_g	3.7
Pinion radius (mm)	r	3.175
Cart velocity threshold value (m/s)		0.025
Cart friction coefficient	μ	0.01
Motor saturation voltage (V)		± 5

obtain comparable decay rates. A list of system parameters is given in Table 1. The numerical and experimental results of Fig. 5 are shown to be in very close agreement, which validates the theoretical model adopted herein. The experimental slosh frequency is slightly lower than the simulated result, and this can be attributed in part to the inertia of the float. The float is lifted up by rising water levels, whereas it falls due to gravity for decreasing water levels, and this creates a lag in the response of the float to water level changes.

4. Input shaping design using optimization

Once a dynamic model has been formulated, an optimization scheme will now be designed to obtain the input shaper parameters, namely the timing and magnitudes of the necessary commanded pulses that drive the system from one point to another while achieving certain prescribed time domain performance specifications. The methodology of input shaper design by optimization adopted herein is also based on the work of Meshreki [9] and Singhose et al. [13]. Although input shaping design is a straightforward procedure in the case of linear systems, the presence of nonlinearities complicates this process. While sloshing may fairly be modeled to be linear, the coupling of sloshing in the present application with the tank's motion, together with the saturation nonlinearity inherent in the motor model, precludes the trivial linear solution, as illustrated by Aboel-Hassan [20]. The methodology of input shaper design by optimization proved to be simple and successful and can be summarized as follows:

(1) A shaper is suggested by the optimization scheme.
(2) The equations governing the system dynamics are numerically integrated based on the shaper parameters to return the time history response of the water.
(3) The performance of the shaper is evaluated using a certain performance index.
(4) The performance index (or objective function value in optimization) is returned to the optimization scheme to decide the next shaper parameters, and hence optimum shaper parameters can be evaluated.

4.1. ZV input shaper for sloshing

Because the ZV shaper has only two variables, namely the time of the second impulse and the amplitude of the first impulse, these can be evaluated by enumeration of all possible combinations in the feasible range and selecting the best results by searching for the minimum value of the performance index. For simplicity, the performance index is taken to be the maximum water slosh level reached after the application of the second impulse. The feasible range and the incremental steps of the enumeration should be based on the specifics of the problem at hand. In this study, the value of the enumeration step of the second impulse timing (T_2) is taken equal to the digital resolution of the experimental controller which was 0.01 s.

The maximum amplitude of the residual sloshing is more sensitive to changes in the second impulse timing (T_2) than changes in the amplitude of first impulse (A_1). This is predicted since input shaping is generally more sensitive to parameters dependent on the natural frequency of the system (T_2 in this case) than to parameters dependent on the damping ratio (A_1 in this case). This is evident from Fig. 6, which shows a 3D plot of the residual slosh amplitude versus T_2 and A_1. The slope along the A_1 direction is relatively smoother than the one along the T_2 direction.

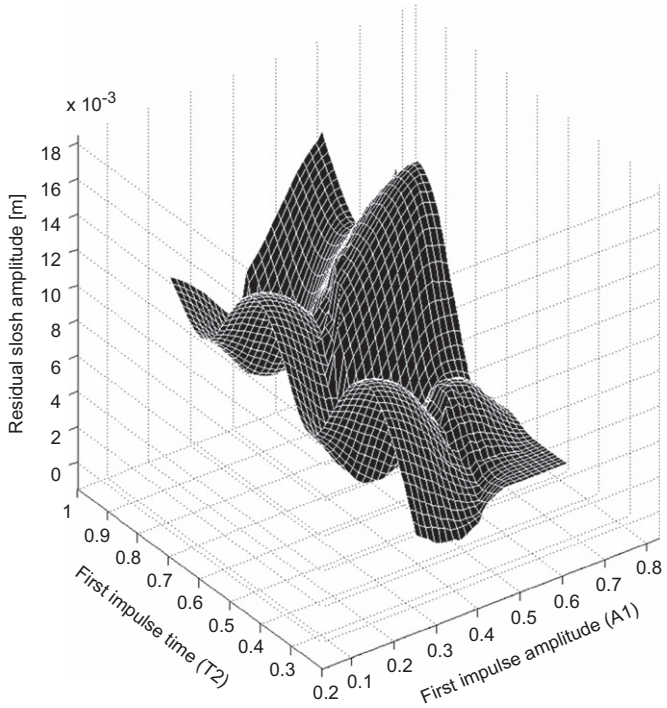

Fig. 6. Residual slosh amplitude versus ZV input shaper parameters.

The experimental results of the ZV shaper designed based on enumeration are shown in Fig. 7 and the optimum shaper parameters are $A_1 = 0.4$, $T_2 = 0.52$ for a shaper designed for a liquid of 4 cm while the final desired cart displacement is 0.6 m. The plot shows both the shaped and unshaped responses for comparison. The maximum residual slosh amplitude after the motor settles in the unshaped case is 0.92 cm. This value is reduced to 0.16 cm (82% reduction in residual amplitude) after applying the input shaper. The reduction in the residual slosh amplitude comes at the cost of increasing the motor settling time, as shown in Fig. 8, from 1.01 s for the unshaped case to 1.34 s for the shaped case. The unusual result of the second impulse being larger than the first impulse is in fact due to the combined effects of saturation and the 1 s search space limit imposed on the second impulse. Because of motor saturation, the cart is incapable of reaching 50% of the final position fast enough to catch the water wave in correct timing to give a destructive second impulse; therefore, the motor has to stand still for nearly another slosh cycle before applying the second impulse. However, since a 1 s limit is imposed on the time of the second impulse, this solution is not included in the search space, and the next best solution turned out to be for $A_1 = 0.4$.

It is interesting to examine the frequency spectra of the residual sloshing of the unshaped and shaped responses shown in Fig. 9, since input shaping is essentially a filtering technique. Inspection of Fig. 9 reveals that the fundamental sloshing mode is significantly suppressed by the input shaper. The second and third sloshing modes, which appear clearly in the unshaped response, are not as considerably attenuated. The fact that the input shaper succeeded in suppressing mainly the fundamental mode, and not the higher modes, is expected since the ZV shaper has only two impulses, thus only one mode can be suppressed at a time. Since the fundamental sloshing mode is the dominant wave in the unshaped response, the optimization scheme gave the shaper that would suppress that mode only. Multi-mode shapers are mentioned repeatedly in the literature [21–24] and can be designed easily by increasing the degrees of freedom of the shaper. In the present application, however, the fundamental slosh mode was practically the most dominant, thus its attenuation was sufficient to reduce most of the undesirable residual sloshing of the liquid.

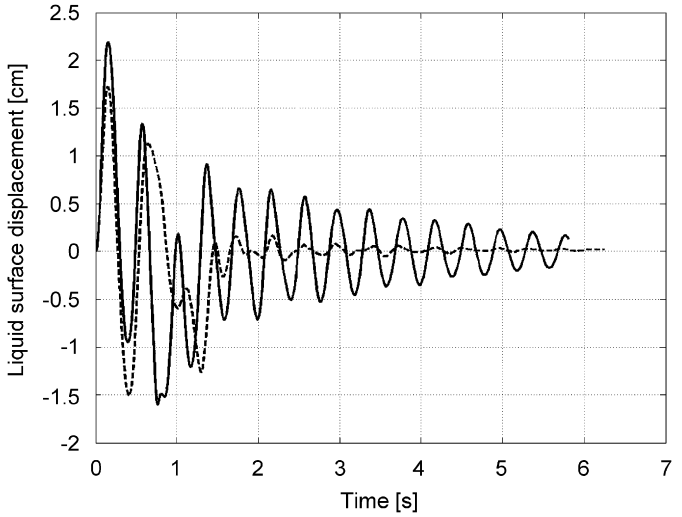

Fig. 7. Experimental ZV shaper performance as indicated by the liquid surface displacement: — unshaped; – – – shaped.

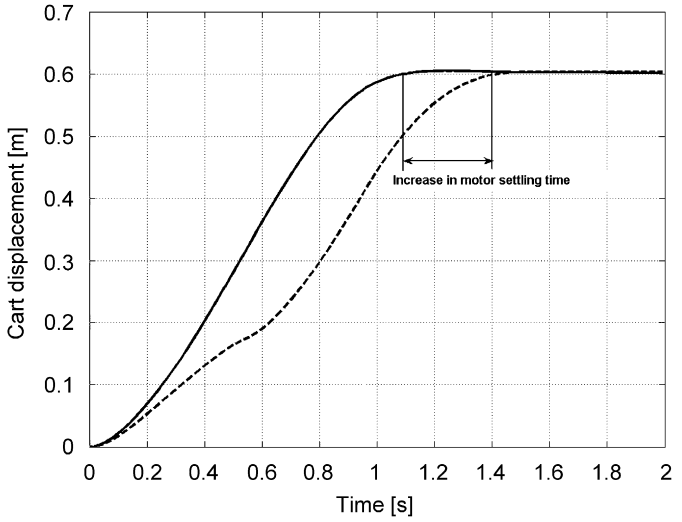

Fig. 8. Experimental cart response for: — unshaped and – – – shaped commands showing an increase in motor settling time ($x_{\text{final}} = 0.6$ m, $K_p = 25$, $h_0 = 4$ cm).

4.2. Higher order input shaper for improved robustness

While the main advantage of the ZV input shaper is the simplicity of the design procedure, this comes at the cost of increased sensitivity to modeling errors or parameters variation. As shown in Ref. [1] for a second-order system, input shaper performance degrades sharply for a change of the natural frequency of a mere $\pm 3\%$. Linear ZV shapers are more sensitive to errors in the natural frequency than they are to errors in the damping ratio. For the case at hand, a tank filled with water up to a height of 4 cm has a fundamental slosh frequency of 2.58 Hz. While this value will increase and saturate at 2.79 Hz (8.1% increase) for appreciably high water heights, it will drop sharply for smaller heights, as shown in Fig. 10. Consequently, a linear ZV shaper is expected to give inferior performance if designed at a water height of 4 cm and operates at smaller heights. This is indicated in Fig. 11 which shows the numerically simulated residual vibration amplitude when applying the optimum ZV shaper designed for a height of 4 cm to operating water heights varying from 50% to 300% of the design height. The ratio of operating to design liquid height is denoted as the non-dimensional

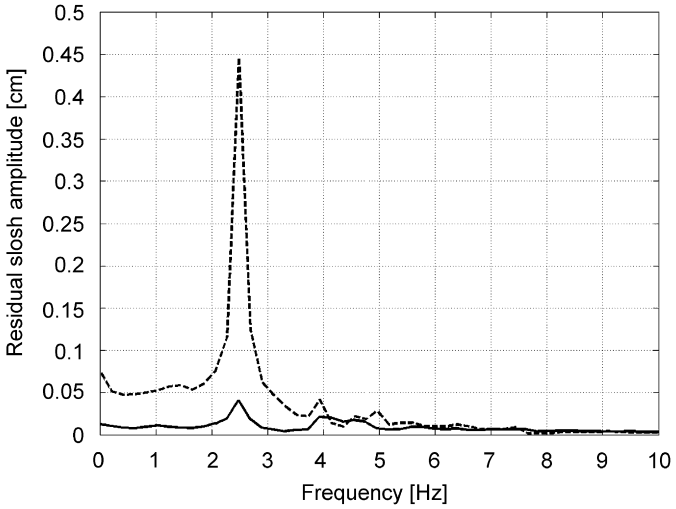

Fig. 9. Residual slosh spectra for: – – – unshaped, and — shaped response for ZV shaper.

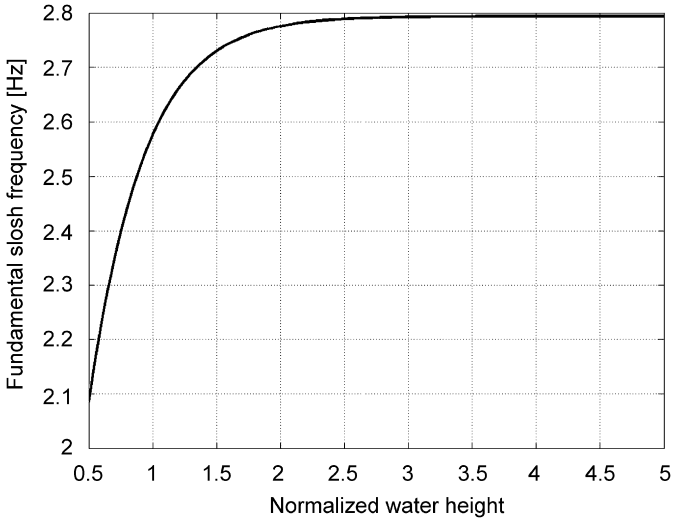

Fig. 10. Effect of water height on the fundamental slosh frequency.

liquid height and is shown in the abscissa. The minimum value of residual slosh amplitude is at a non-dimensional height of unity, as expected. The curve almost saturates for values greater than 1 while it shoots up for values less than 1.

The problem of shaper sensitivity has been tackled in the literature by adding an extra constraint in the design of the shaper in addition to the traditional ZV constraint. For example, in a Zero Vibration Derivative (ZVD) shaper [1], the additional constraint is to set the derivative of the residual vibration with respect to a certain model parameter, typically the natural frequency, to zero resulting in a shaper having 3 pulses. Extra-Insensitive (EI) shapers [2] and shapers with Specified Insensitivity (SI) [3] are other types of robust input shapers with even more insensitivity to parameter variation and modeling errors. As in ZVD, EI and SI shapers increase the degrees of freedom of the ZV shaper by adding another impulse, while placing different constraints on the solution. A similar strategy to EI and SI shaper design will be adopted in this work to design a robust input shaper for the present application. The four variables of the input shaper preclude the use of enumeration to determine the optimum shaper; therefore, a more elaborate optimization scheme is employed. Because of the limited number of variables, and the expected harmonic nature of the objective function, it was

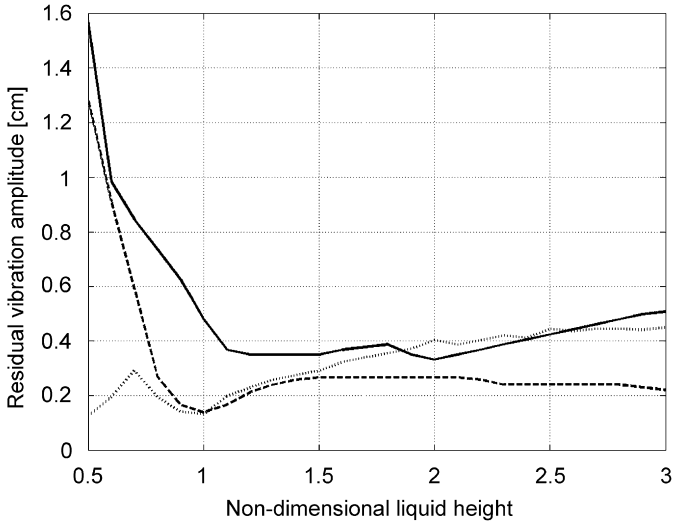

Fig. 11. Residual vibration amplitude: — unshaped; – – – ZV; and ····· robust responses. Shapers are designed for a liquid height of 4 cm ($x_{\text{final}} = 0.6$ m, $K_p = 25$).

Table 2
GA basic parameters used in optimization

Number of variables	4
Population size	60
Number of generations	40
Uniform mutation	4
Boundary mutation	4
Arithmetic cross over	2
Simple arithmetic	2
Whole non-uniform mutation	4
Heuristic cross-over	2
None uniform mutation parameter	6
Simple cross-over parameter	10
Q	0.1

decided to use real-coded GA [25], since local search methods are likely to get 'trapped' in one of the local minima and miss the global minimum.

There are mainly two challenges in optimization problems. First, to transform the qualitative design requirements into a quantitative performance index, in order to be able to state an objective function that captures all the elements of the design requirements. Second, the optimization scheme itself has to be fine-tuned based on the characteristics of the problem at hand. The various parameters employed in the present GA scheme are listed in Table 2.

The qualitative design requirements of the improved shaper are:

(1) creating minimum residual vibration at the design water height.
(2) should the water height decrease, the shaper has to remain effective in suppressing the residual vibration.
(3) the shaper time should be minimal to avoid the trivial solution of achieving good residual amplitude response at the cost of increasing the motor settling time indefinitely.

The first requirement is represented by the largest magnitude of the residual sloshing after the settling of the motor, hence its objective function is stated as

$$\text{obj}_1 = \max(U_{t=T_s}^{t=T_f}) \quad \text{at } h_{\text{operating}} = h_{\text{design}} \tag{15}$$

where U is the displacement of the surface liquid node adjacent to the tank wall in the FE model, T_s is the settling time of the motor and T_f is the final time value. This objective is taken for the case where the water level in the tank, $h_{\text{operating}}$, is equal to the water height at which the shaper is designed, h_{design}.

The second design requirement stated above has to do with the robustness of the shaper. From Fig. 11, it is evident that the ZV shaper performance, as measured by the residual vibration amplitude, deteriorates significantly in the region where the non-dimensional height is from 50% to 75%. The aim of designing a robust shaper is to improve insensitivity by reducing such a sharp slope. Considering the specifics of the problem at hand, and the fact that it is explicitly desired to reduce the sensitivity of the sloshing in the direction of decreasing operating heights, it becomes evident that an improved shaper can be designed by frequency sampling, as in SI shaper design. To this end, the second requirement's objective function is expressed in a similar form as the previous case with the response sampled at two operating heights lower than the design height:

$$\text{obj}_2 = \max(U_{t=T_s}^{t=T_f})_{h_{\text{operating}}=0.5h_{\text{design}}} + \max(U_{t=T_s}^{t=T_f})_{h_{\text{operating}}=0.75h_{\text{design}}} \tag{16}$$

The third design requirement dealing with the settling time of the motor is represented by the increase of the settling time of the motor (T_s) in the shaped command compared to the unshaped command, and is expressed as

$$\text{obj}_3 = \max(T_{s(\text{shaped})} - T_{s(\text{unshaped})}) \tag{17}$$

In order to add the objective functions algebraically, they all must have comparable magnitudes, so that no one objective dominates the others. This can be done by normalizing the three objectives and adding factors to the normalized objective function to allow the designer to give different weights for each objective. The objective function is finally expressed as

$$\text{obj} = \sum_{i=1}^{3} k_i \times \frac{\max(U_{t=T_s}^{t=T_f})_{\text{shaped}}@h = c_i \times h_{\text{design}}}{\max(U_{t=T_s}^{t=T_f})_{\text{unshaped}}@h = c_i \times h_{\text{design}}} + k_4 \frac{(T_{s(\text{shaped})} - T_{s(\text{unshaped})})}{T_{s(\text{unshaped})}} \tag{18}$$

where k_i is the weighting factor for each design criterion, h is the operating height, h_{design} is the water height at which the shaper is designed, c_i are factors taken as [1,0.75,0.5]. The dashed and dotted plots of Fig. 11 show numerical run of the sensitivity of the ZV and robust shapers, respectively, for non-dimensional heights ranging from 0.5 to 3 together with the performance of the unshaped response. The optimum shaper parameters for this case are $A_1 = 0.2$, $A_2 = 0.19$, $T_2 = 1.02$ and $T_3 = 1.22$. The weighting factors used in the objective function of the robust shaper are $k_1 = 3$, $k_2 = 2$, $k_3 = 2$, $k_4 = 1$. It is clear that the ZV and robust shapers are both superior to the unshaped command over almost the entire range of operation. It is also clear that the designed robust shaper was successful in reducing the residual vibration amplitude significantly for non-dimensional heights in the range of 0.5–0.75. The use of the robust shaper is particularly advantageous in practical applications where a drop in natural frequency is likely to occur as the liquid being transported is periodically consumed or dispensed. This improvement in the performance comes at the cost of deteriorating performance for higher non-dimensional heights; however, it still remains below the unshaped command response. This deterioration is expected since no factor in the objective function reflects the performance of the proposed robust shaper in that range. The improvement comes at the cost of increased motor settling time as well. Fig. 12 shows a numerical comparison of the unshaped, ZV and robust shaper responses where the input shapers are designed for a water height of 4 cm while the actual height is 3 cm. The least residual vibration is observed for the robust shaper, as intended.

4.3. Deflection limiting (DL) input shaper for sloshing

The convenience of the numerical model and shaper design using optimization techniques make the addition of more objectives and motion constraints very attractive. One constraint repeatedly addressed in the literature is DL [13] in which the maximum magnitude of structural deflection is limited to a certain predefined value. This constraint is useful for applications that involve partially filled moving tanks since it may be desired to prevent spilling during motion.

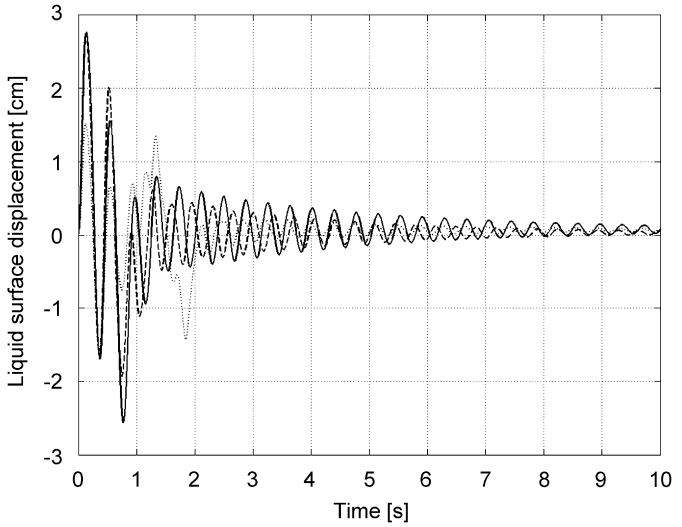

Fig. 12. Numerical comparison of — unshaped; – – – ZV; and ····· robust shaper responses ($x_{\text{final}} = 0.6\,\text{m}$, $K_p = 25$, $h_0 = 4\,\text{cm}$, $h_{\text{operating}} = 3\,\text{cm}$).

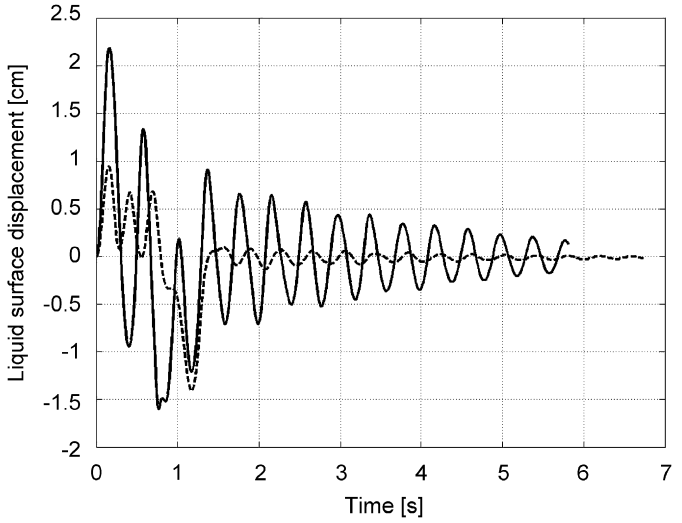

Fig. 13. Experimental response: — unshaped; – – – DL shaper ($x_{\text{final}} = 0.6\,\text{m}$, $K_p = 25$, $h_0 = 4\,\text{cm}$).

In the optimization scheme, DL can be expressed as a constraint, where a penalty is applied to the objective function should the maximum amplitude of vibration of any of the FE nodes exceeds a predefined value. Since DL is a hard constraint, the weighting factors suggested in Eq. (18) have to be chosen carefully to relax other objectives in favor of the constraint. For example, it is expected that the DL constraint would cause the settling time of the motor to increase. Physically, this means that requiring fast motor maneuvers with limited liquid slosh are two contradicting objectives, thus one of them has to be relaxed to be able to accomplish the other. In the experimental run shown in Fig. 13, the maximum positive amplitude of vibration was limited to 1 cm. The optimum shaper parameters for this case are $A_1 = 0.167$, $A_2 = 0.22$, $T_2 = 0.22$ and $T_3 = 0.44$ and the weighting factors used in Eq. (18) are $k_1 = 3$, $k_2 = 1$, $k_3 = 1$ and $k_4 = 0.5$. Comparing the DL response of Fig. 13 with the unshaped response in Fig. 7 indicates that the adopted input shaping technique can successfully reduce the maximum amplitude of sloshing from 2.3 to 0.95 cm and reduce the maximum residual sloshing from 0.9 to 0.15 cm. The improved performance comes at the mere cost of 0.42 s increase in the motor rise time [20].

5. Conclusions

This work demonstrated both theoretically and experimentally how input shaping techniques can effectively be applied to mitigate sloshing effects in open liquid tanks undergoing point-to-point maneuvers. The system dynamics were modeled numerically, taking into consideration motor saturation and friction. The input shaper parameters were optimized to find the commands that would result in minimum residual vibration. The objectives were to minimize residual vibration, as well as the motor settling time. The two main input shaping techniques addressed in this work were the ZV and robust shaper schemes. Both demonstrated improved performance over unshaped commands. While ZV was capable of reducing residual vibration by nearly 80%, its sensitivity was outperformed by the robust shaper, which showed a larger range of acceptable performance allowing more room for modeling errors and parameter variation. The concept of DL, originally developed in the literature to minimize structural swaying during commanded motion, was implemented herein to limit the amplitude of liquid sloshing over the entire length of the tank motion, thus reducing the chances of spilling.

References

[1] N.C. Singer, W.P. Seering, Preshaping command inputs to reduce system vibration, *Journal of Dynamic Systems, Measurement and Control* 112 (1990) 76–82.
[2] W. Singhose, W. Seering, N. Singer, Residual vibration reduction using vector diagrams to generate shaped inputs, *Journal of Mechanical Design* 116 (2) (1994) 654–659.
[3] W.E. Singhose, W.P. Seering, N.C. Singer, Input shaping for vibration reduction with specified insensitivity to modeling errors, *Proceedings of the Japan/USA Symposium on Flexible Automation* 1 (1996) 307–313.
[4] C.F. Cutforth, L.Y. Pao, Adaptive input shaping for maneuvering flexible structures, *Automatica* 40 (2004) 685–693.
[5] M. Bodson, An adaptive algorithm for the tuning of two input shaping methods, *Automatica* 34 (6) (1998) 771–776.
[6] H. Kojima, W. Singhose, Adaptive deflection-limiting control for slewing flexible space structures, *Journal of Guidance, Control and Dynamics* 30 (1) (2007) 61–67.
[7] K. Sorensen, W. Singhose, Oscillatory effects of common hard nonlinearities on systems using two-impulse ZV input shaping, *Proceedings of the 2007 American Control Conference* (2007) 5539–5544.
[8] J. Lawrence, K. Hekman, W. Singhose, An analytical solution for a zero vibration input shaper for systems with coulomb friction, *Proceedings of the 2002 American Control Conference* 5 (2002) 4068–4073.
[9] M.A.H. Meshreki, Design Methodology for Input Shapers Using Genetic Algorithms in Flexible Nonlinear Systems, Masters Thesis, American University in Cairo, Egypt, 2004.
[10] Z. Mohamed, M.O. Tokhi, Hybrid control schemes for input tracking and vibration suppression of a flexible manipulator, *Proceedings of the Institution of Mechanical Engineers, Part I, Journal of Systems and Control Engineering* 217 (1) (2003) 23–34.
[11] K. Sorensen, W. Singhose, S. Dickerson, A controller enabling precise positioning and sway reduction in bridge and gantry cranes, *Control Engineering Practice* 15 (2007) 825–837.
[12] K. L. Sornesen, A Combined Feedback and Command Shaping Controller for Improving Positioning and Reducing Cable Sway in Cranes, Masters Thesis, Georgia Institute of Technology, USA, 2005.
[13] W. Singhose, A. Banerjee, W. Seering, Slewing flexible spacecraft with deflection-limiting input shaping, *Journal of Guidance, Control, and Dynamics* 2 (1997) 291–298.
[14] A.K. Banerjee, Dynamics and control of the wisp shuttle-antennae system, *Journal of Astronautical Sciences* 1 (1993) 73–90.
[15] T. Miyoshi, Y. Noda, K. Terashima, Feedforward control considering input and states constraints with eliminating residual vibration, *Proceedings of the 2007 American Control Conference* (2007) 5005–5010.
[16] K. Terashima, K. Yano, Sloshing analysis and suppression control of tilting-type automatic pouring machine, *Control Engineering Practice* 9 (2001) 607–620.
[17] J. Feddema, C. Dohrmann, G. Parker, R. Robinett, V. Romero, D. Schmitt, A comparison of maneuver optimization and input shaping filters for robotically controlled slosh-free motion of an open container of liquid, *Proceedings of the 1997 American Control Conference* 3 (1997) 1345–1349.
[18] N. Singer, W. Singhose, W. Seering, Comparison of filtering methods for reducing residual vibration, *European Journal of Control* 5 (1999) 208–218.
[19] M. Arafa, Finite element analysis of sloshing in rectangular liquid-filled tanks, *Journal of Vibration and Control* 13 (7) (2007) 883–903.
[20] A. Aboel-Hassan, Design and Optimization of Input Shapers for Liquid Slosh Suppression, Masters Thesis, American University in Cairo, Egypt, 2007.
[21] G. Cook, Control of flexible structures via posicast, *Proceedings of the Eighteenth Southeastern Symposium on System Theory* (1986) 31–35.
[22] J.M. Hyde, W.P. Seering, Inhibiting Multiple Mode Vibration in Controlled Flexible Systems, *Proceedings of the 1991 American Control Conference* 3 (1991) 2449–2454.

[23] J.M. Hyde, W.P. Seering, Using input command pre-shaping to suppress multiple mode vibration, *Proceedings of the IEEE International Conference on Robotics and Automation* 3 (1991) 2604–2609.
[24] W. Singhose, E. Crain, W. Seering, Convolved and simultaneous two-mode input shapers, *IEE Proceedings: Control Theory and Applications* 144 (1997) 515–520.
[25] F. Herrera, M. Lozano, J.L. Verdegay, Tackling real-coded genetic algorithms: operators and tools for behavioral analysis, *Artificial Intelligence Review* 12 (1998) 265–319.